Icarus 212 (2011) 339–350

Contents lists available at ScienceDirect

Icarus

journal homepage: www.elsevier.com/locate/icarus

Uranus' cloud structure and seasonal variability from Gemini-North and UKIRT observations

P.G.J. Irwin [a,*], N.A. Teanby [b], G.R. Davis [c], L.N. Fletcher [a], G.S. Orton [d], D. Tice [a], A. Kyffin [a]

[a] Atmospheric, Oceanic, and Planetary Physics, Department of Physics, University of Oxford, Clarendon Laboratory, Parks Rd., Oxford OX1 3PU, United Kingdom
[b] Department of Earth Sciences, University of Bristol, Wills Memorial Building, Queen's Road, BRISTOL BS8 1RJ, United Kingdom
[c] Joint Astronomy Centre, 660 N. A'ohoku Place, Hilo, HI 96720, USA
[d] Jet Propulsion Laboratory, California Institute of Technology, 4800 Oak Grove Drive, Pasadena, CA 91109, USA

ARTICLE INFO

Article history:
Received 25 October 2010
Revised 17 December 2010
Accepted 19 December 2010
Available online 28 December 2010

Keywords:
Atmospheres, Composition
Uranus
Uranus, Atmosphere
Atmospheres, Dynamics
Data reduction techniques

ABSTRACT

Observations of Uranus were made in September 2009 with the Gemini-North telescope in Hawaii, using both the NIFS and NIRI instruments. Observations were acquired in Adaptive Optics mode and have a spatial resolution of approximately 0.1″.

NIRI images were recorded with three spectral filters to constrain the overall appearance of the planet: J, H-continuum and CH_4(long), and long slit spectroscopy measurements were also made (1.49–1.79 μm) with the entrance slit aligned on Uranus' central meridian. To acquire spectra from other points on the planet, the NIFS instrument was used and its 3″ × 3″ field of view stepped across Uranus' disc. These observations were combined to yield complete images of Uranus at 2040 wavelengths between 1.476 and 1.803 μm.

The observed spectra along Uranus central meridian were analysed with the NEMESIS retrieval tool and used to infer the vertical/latitudinal variation in cloud optical depth. We find that the 2009 Gemini data perfectly complement our observations/conclusions from UKIRT/UIST observations made in 2006–2008 and show that the north polar zone at 45°N has continued to steadily brighten while that at 45°S has continued to fade. The improved spatial resolution of the Gemini observations compared with the non-AO UKIRT/UIST data removes some of the earlier ambiguities with our previous analyses and shows that the opacity of clouds deeper than the 2-bar level does indeed diminish towards the poles and also reveals a darkening of the deeper cloud deck near the equator, perhaps coinciding with a region of subduction. We find that the clouds at 45°N,S lie at slightly lower pressures than the clouds at more equatorial latitudes, which suggests that they might possibly be composed of a different condensate, presumably CH_4 ice, rather than H_2S or NH_3 ice, which is assumed for the deeper cloud. In addition, analysis of the centre-to-limb curves of both the Gemini/NIFS and earlier UKIRT/UIST IFU observations shows that the main cloud deck has a well-defined top, and also allows us to better constrain the particle scattering properties.

Overall, Uranus appeared to be less convectively active in 2009 than in the previous 3 years, which suggests that now the northern spring equinox (which occurred in 2007) is passed the atmosphere is settling back into the quiescent state seen by Voyager 2 in 1986. However, a number of discrete clouds were still observed, with one at 15°N found to lie near the 500 mb level, while another at 30°N, was seen to be much higher at near the 200 mb level. Such high clouds are assumed to be composed of CH_4 ice.

1. Introduction

Uranus is one of the most enigmatic planets of the outer Solar System. Its very high obliquity of 98° is quite unlike that of any other planet we know and Voyager 2, in 1986, found the planet to be in almost perfect thermal equilibrium with the incident solar radiation, unlike all the other giant planets where residual heat from formation or heat released by subsequent fractionation is significantly greater than the amount received from the Sun. The Voyager 2 flyby also revealed an atmosphere which appeared almost completely devoid of the usual banded cloud structure and vortices seen on the other giant planets, although it was concluded that the atmosphere must somehow efficiently redistribute heat from the southern hemisphere, which in 1986 was pointed almost directly towards the Sun, to the winter northern hemisphere, since temperature variations across the planet were found to be surprisingly small (Hanel et al., 1986; Flasar et al., 1987).

* Corresponding author. Fax: +44 1865 272923.
E-mail address: irwin@atm.ox.ac.uk (P.G.J. Irwin).

0019-1035/$ - see front matter © 2011 Elsevier Inc. All rights reserved.
doi:10.1016/j.icarus.2010.12.018

This perception of a featureless planet was not always so. Visual observations by ground-based astronomers have shown the appearance of Uranus to change markedly with Uranus' season (Alexander, 1965) and since 1986, as Uranus has moved towards its northern spring equinox in 2007, this change in appearance has been captured with modern instruments at multiple wavelengths with both ground-based and space telescopes. By the early 1990s a bright zone had appeared at 45°S and discrete clouds began to be observed at southern and later northern mid-latitudes. During the equinox period itself, this bright zone at 45°S was seen to fade and a new zone at 45°N started to form (Irwin et al., 2009, 2010; Sromovsky et al., 2009), while equatorial latitudes also brightened. These observations were used to infer changes in the latitudinal/vertical cloud structure by a number of authors (Irwin et al., 2009, 2010; Sromovsky et al., 2009), using measured near-IR reflectance spectra at wavelengths where the transmission to and from different levels in Uranus' atmosphere is determined by the absorption of methane, which most authors have previously assumed to be vertically well mixed below the condensation level at approximately 1.5 bar, and invariant with latitude. However, Karkoschka and Tomasko (2009) used HST-STIS observations from 2002 at wavelengths dominated by hydrogen absorption to demonstrate that the assumption of constant methane abundance, invariant with latitude, may not be reliable. Instead they found the abundance of methane to be approximately 3–4% at equatorial latitudes, reducing to 1–2% at latitudes polewards of 45°S. In the light of these new methane determinations, Irwin et al. (2010) reanalysed a set of observations made with the UIST instrument on the UK Infrared Telescope (UKIRT) on Mauna Kea, Hawaii between 2006 and 2008 at wavelengths dominated by methane opacity and demonstrated that the latitudinal and seasonal variations of cloud opacity previously determined from these observations were only slightly affected if a variable methane abundance was assumed. The reliability of previous estimations is also dependent on the accuracy of the assumed methane absorption coefficients. Karkoschka and Tomasko (2010) showed that the methane data used by most researchers prior to 2009 had insufficient absorption at wavelengths of weak absorption and published a revised dataset based on existing laboratory measurements and also measurements from the Huygens probe during its descent through Titan's atmosphere in 2005. These new methane absorption data were used by Irwin et al. (2010) in their revised analysis and were shown to move the retrieved pressure level of the main clouds to slightly lower pressures and also to provide much greater consistency between cloud retrievals made in the H-band (1.6 μm) and J-band (1.3 μm).

While the existing UKIRT/UIST observations have been used to good effect to monitor the seasonal development of Uranus' latitudinal–vertical cloud structure, the spectral data were limited to the central meridian. Hence, there remained a degree of uncertainty as to whether the latitudinal variations detected were real or whether they were, in part, an artefact of the increasing zenith angle of the observations towards the poles. Another limitation of the UKIRT long-slit spectral observations is that they have limited vertical resolution. Better vertical resolution can be achieved if the same latitude is observed at a range of zenith angles to determine the centre-to-limb curves. Such an analysis has previously been done with Keck and HST imaging observations (Sromovsky and Fry, 2007) and was found to constrain much better the cloud reflectivity solution. Finally, UKIRT does not have an adaptive optics system and so the spatial resolution is limited to the atmospheric 'seeing' at the summit of Mauna Kea. Resolutions as good as 0.48″ were possible in 2006–2008, but at this level there is still considerable smoothing of the latitudinal variations and also considerable mixing with space for latitudes observed towards the limb, i.e. polar latitudes.

To address these deficiencies and also to extend the seasonal monitoring of Uranus' cloud evolution through its equinox for another year, time was awarded by the Gemini-North telescope in Hawaii in 2009 to observe Uranus with both the NIRI (Near Infra-Red Imager and Spectrometer) and NIFS (Near-Infrared Integral Field Spectrometer) instruments using the ALTAIR adaptive optics system. The NIRI observations were performed to mimic as much as possible the existing UKIRT/UIST observations, while the NIFS observations were designed to observe all observable latitudes over as wide a range of zenith angles as possible and thus determine the centre-to-limb curves at multiple wavelengths. In this paper we will describe these new observations and examine what they reveal about continuing seasonal changes. We shall also examine what the improved spatial resolution of the dataset implies for the vertical cloud distribution, in particular by studying the observed NIFS centre-to-limb curves.

2. Observations

The Gemini-North observations were made in September 2009 using the ALTAIR adaptive optics system and both the NIRI and NIFS instruments. The ALTAIR adaptive optics (AO) system needs a guide 'star' to provide wavefront correction and since Uranus moves with respect to the celestial sphere, some of Uranus' moons were instead used as guide 'stars', with Titania and Ariel proving to be the most suitable targets. Using this system, we were able to obtain observations with a spatial resolution of 0.1″, a considerable improvement on our existing UKIRT/UIST non-AO observations, which had a spatial resolution of 0.48″.

NIRI observations were made in both imaging and spectroscopy modes. Images were recorded at $f/32$ (0.02″/pixel plate scale) with three filters: J, H-continuum and CH_4(long) (Table 1). The appearance of Uranus on 18th September 2009 in these three channels is shown in Fig. 1. Both the J and H-continuum filters are sensitive to sunlight reflected from levels as deep as ~8 bars, while the CH_4(long) filter is only sensitive to light reflected from clouds/hazes above the 0.5-bar level. Comparing the J and H-cont images we see the same general features, but the contrast of the J-band image is more muted. Since the opacity of small haze particles increases roughly as $1/\lambda^4$, if we assume the Rayleigh limit for conservatively scattering particles, then we might expect an increase in overlying haze opacity of $(1.58/1.3)^4 = 2.2$ from H-band to J-band. From the CH_4(long) filter we can see that any haze is approximately uniformly distributed, with similar limb-brightening at all latitudes (although the haze seems slightly thicker over the equator, perhaps related to the infall of ring material (Karkoschka and Tomasko, 2009) and also towards each pole) and so we conclude that the suppressed contrast in the J filter image is due to increased obscuration by this overlying haze at shorter wavelengths. The CH_4(long) filter image also clearly shows the position of the ring and from this we can see that the slight darkening seen near the equator of the J and H-cont images does not quite coincide with the ring and thus that this feature is due to actual variations in opacity of the deeper cloud decks, rather than simply a geometrical effect of ring obscuration. The same set of images recorded on 25th September 2009 (Fig. 2) shows the same overall features, albeit with slightly poorer spatial resolution. Fig. 2 also shows a number

Table 1
Gemini-N/NIRI imaging filters used in this study.

Filter	Central wavelength (μm)	Range (μm) or $d\lambda/\lambda$
J	1.25	1.15–1.33
H-continuum	1.57	1.5%
CH_4(long)	1.69	6.5%

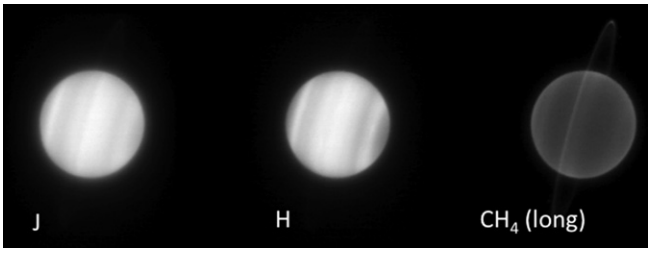

Fig. 1. Gemini-N/NIRI images of Uranus on 18th September 2009 in filters: J (left), H-continuum (centre) and CH_4-long (right). Here the NIRI focal plane was aligned N–S with respect to the celestial sphere and so Uranus' north pole is at the lower right of these images. A thin dark region can be seen at Uranus' equator in both the J and H-continuum images (at wavelengths where Uranus' atmospheric methane is poorly absorbing allowing reflection to be observed from cloud particles deep in Uranus' atmosphere) as well as a darkening just equatorwards of the bright zones at 45°N,S.

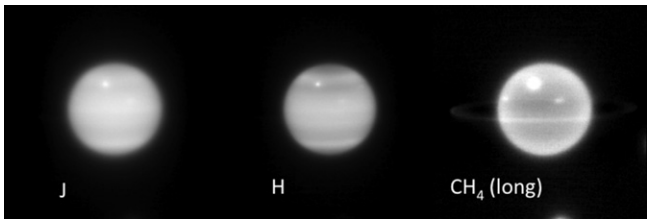

Fig. 2. Gemini-N/NIRI images of Uranus on 25th September 2009 in filters: J, H-continuum and CH_4-long. On this occasion the NIRI focal plane was aligned to Uranus' central meridian so the north pole is at the top. A number of small discrete cloud features can be seen in Uranus' northern hemisphere.

of small discrete cloud features, one of which, just south of the 45°N cloud zone is visible in all three filters showing it to have much greater opacity than two other features at lower northern latitudes, which are only clearly discernable in the CH_4(long) filter. It is not possible to determine if these storms had arisen since the previous NIRI observations on 18th September 2009 since, using the Uranus wind speed profile of Hammel et al. (2001) we calculate that they would have appeared on the far side of Uranus during the earlier NIRI observation.

In addition to these NIRI images, long slit spectra were made in the H-band, also at *f*/32 (0.02″/pixel), with the 4-pixel-wide slit aligned on the planet's central meridian and the planet nodded up and down the slit by a distance of 8″. Spectra were recorded over the range 1.49–1.79 μm at a spectral resolution of $R = 880$ (Table 2).

The main observation time on Gemini-North was devoted to observing Uranus with the NIFS instrument, which is an Integral Field Unit (IFU) spectrometer. This instrument is able to provide mapping spectrometry and returns images at 2040 wavelengths from a scene covering approximately 3″ × 3″, with a pixel scale of 0.103″ across slices and 0.043″ along slices. NIFS observations were made using the H-grating and cover the wavelength range 1.476–1.803 μm, with a spectral resolution of $R = 5290$ (Table 3). Since Uranus' disc is larger than the NIFS FOV, observations were made with the FOV dithered across the planet, and these 'frames' were then recombined using the telescope tracking data, and the planet edge and epsilon ring as reference markers. Between each Uranus integration of 2 min the FOV was switched to record dark space for the same length of time, in order to provide the background Earth atmospheric emission correction. Although the NIFS observations have very high resolving power, this comes at the expense of increased noise. In addition, the laboratory measurements on which the current absorption k-table for methane is based (Irwin et al., 2006; Karkoschka and Tomasko, 2010), have a spectral resolution of 10 cm^{-1}, which equates to a spectral resolving power (at 1.57 μm) of 640. Hence, we are unable at present to make full use of the higher spectral resolution of the NIFS instrument. Instead, for consistency with earlier UKIRT/UIST observations the observations were smoothed with a triangular instrument function of FWHM = 0.004 μm and tabulated at a spacing of 0.001 μm. This meant that the data could be used directly with the *k*-tables previously generated from the Karkoschka and Tomasko (2010) dataset and used by Irwin et al. (2010) to reanalyse the UKIRT/UIST observations. This table has a spectral resolution $R = 392$ at 1.57 μm.

To correct for telluric transmission, observations were also made (for both NIFS and NIRI) of a standard star, for which we chose HIP115119 (A0V type, RA: 23:19:02.148, Dec: −12:10:13.53), which was reasonably close to the position of Uranus during this apparition (Uranus' position on 25th September 2009 was RA: 23:39:53.52, Dec: −03:02:42.80).

In addition to the 2009 Gemini-North observations, we also report here UKIRT observations made on 25th July 2008 using the UIST instrument in its IFU mode. Just like the Gemini/NIFS instrument, in its IFU mode UIST simultaneously forms spectra from a number of slits across the target, giving a total FOV of 3.3″ × 6″ and a plate scale of 0.24″ × 0.12″, i.e. 0.12″ along slit and 0.24″ across slit. Again, the FOV was slightly too small to cover the entire Uranus' disc and so data were recorded of first the northern and then the southern hemisphere, with the highest spatial resolution aligned in the E–W direction to achieve the best sampling of the centre-to-limb curves at different latitudes (Table 4). The spectra were recorded using the HK grism and have the same wavelength range as UIST long slit spectra, but twice the spectral resolution (1.395–2.506 μm, $R = 1000$). The total on-planet integration time of these observations was 16 min per hemisphere and again an equal amount of time was spent observing space to properly correct for atmospheric emission. Telluric correction was achieved through measurements of the UKIRT standard star: BS8931 (HD 221356 – RA: 23:31:31.503, Dec: −04:05:14.66).

The UKIRT UIST data were reduced using the UKIRT facility software (Cavanagh et al., 2008), while the Gemini observations were reduced using Gemini-IRAF (Tody, 1993).

3. Seasonal variations

We found the Gemini/NIFS data to be of higher seeing quality than the Gemini/NIRI spectral observations and so, once the different NIFS observations had been combined together as previously described, the spectra along the central meridian of the NIFS

Table 2
Summary of Gemini-N/NIRI Uranus observations in the 2009 campaign.

Date (YYYYMMDD)	Grism/filter	T-start	T-end	Integration time
20090918	J	07:39:10	07:43:30	100 s
20090918	H-cont	07:49:52	08:06:22	200 s
20090918	CH_4-long	07:43:30	07:49:52	200 s
20090925	J	08:05:44	08:10:05	100 s
20090925	H-cont	08:16:31	08:22:41	200 s
20090925	CH_4 long	08:10:05	08:16:31	200 s
20090925	H grism	07:21:57	08:00:08	24 m

Table 3
Summary of Gemini-N/NIFS Uranus observations in the 2009 campaign.

Date (YYYYMMDD)	T-start	T-end	Integration time
20090902	10:25:26	11:16:01	18 m (2 m × 9 frames)
20090903	09:15:42	10:11:05	20 m (2 m × 10 frames)
20090904	09:28:51	10:23:54	20 m (2 m × 10 frames)

Table 4
Summary of the UKIRT/UIST IFU observations in 2008.

Date (YYYYMMDD)	T-start	T-end	Integration time
20080725	13:02:41	13:35:41	16 m – S. Hemisphere
20080725	13:38:55	14:11:55	16 m – N. Hemisphere

observations were extracted and used to determine the variation of vertical cloud structure with latitude in 2009 in exactly the same way as with the UKIRT/UIST observations from 2006–2008 (Irwin et al., 2010), using the retrieval tool NEMESIS (Irwin et al., 2008).

Fig. 3 shows the appearance of Uranus in these recombined NIFS observations at a number of wavelengths, which sound progressively deeper levels of Uranus' atmosphere (1.637, 1.622, 1.607, 1.577, 1.592 μm) on the three days of observations (September 2–4th, 2009). The transmission curves to and from space at these wavelengths for nadir viewing are also shown in Fig. 3. Spectra were extracted along the central meridian, smoothed as described earlier, and then sampled at 100 wavelengths between 1.45 and 1.75 μm. The Gemini/NIFS data have much better spatial sampling than the UKIRT/UIST data and thus there were 77 points along the central meridian, compared with 30 points measured with UKIRT/UIST. In addition, the improved spatial resolution meant that there was much less mixing with space for latitudes polewards of 60°N, 60°S, giving the retrievals at more polar latitudes much improved reliability. The improved spatial resolution also meant that there was no longer any need to average the spectra over the zenith angles observed by the FOV, as had to be done for UKIRT/UIST observations, and thus a single zenith angle was used for each latitude, calculated at the centre of the FOV. Fig. 4 shows the reflectivity observed by Gemini/NIFS on 2nd September 2009 along the central meridian, averaged from 1.561 to 1.583 μm (i.e. the UIST H-continuum filter), compared with the previous observations from 2006–2008 made by UKIRT/UIST. The data from 2nd September 2009 were chosen since these were recorded in the orientation that best sampled the N/S variation. It can be seen from Fig. 4 that the seasonal variation seen by UKIRT is clearly continuing, with the southern bright zone at 45°S fading and its counterpart zone at 45°N brightening, and that the Gemini observations with adaptive optics clearly have superior spatial resolution.

These observed spectra along Uranus' central meridian were fitted with our NEMESIS retrieval model (Irwin et al., 2008) to retrieve the vertical profile of cloud opacity as a function of latitude as described by Irwin et al. (2010). The NEMESIS retrieval model uses a correlated-*k* radiative transfer model and minimises the difference between the modelled and measured spectrum using the technique of Optimal Estimation (Rodgers, 2000). The methane absorption coefficients of Karkoschka and Tomasko (2010) were used in this model, together the H_2–H_2 and H_2–He collision induced absorption coefficients of Borysow (1991, 1992) and Zheng and Borysow (1995). An equilibrium ortho/para H_2-ratio was assumed at all altitudes and latitudes. As with our previous analyses, the temperature profile at all latitudes was set to the 'D' profile of Lindal et al. (1987) and extended to higher pressures in the troposphere assuming a saturated adiabatic lapse rate. The abundance of methane was set to 1.6% at all latitudes, with a relative humidity of 30% above the condensation level at approximately 1.2 bars.

Retrievals from the Gemini/NIFS observations from 2nd September 2009 are compared with the retrievals from the UKIRT/UIST observations from 2006–2008 in Fig. 5. The quality of the fit to the Gemini/NIFS observations at a number of latitudes is shown in Fig. 6, together with the broader latitudinal variation of the quality of fit factor, χ^2/n, where n is the number of spectral points, $\chi^2 = \sum_{i=1}^{n}((y_i - m_i)/\sigma_i)^2$, and y_i are the fitted spectral radiances, m_i are the observed radiances and σ_i are the errors of these measured radiances. It can be seen that at most latitudes, the value

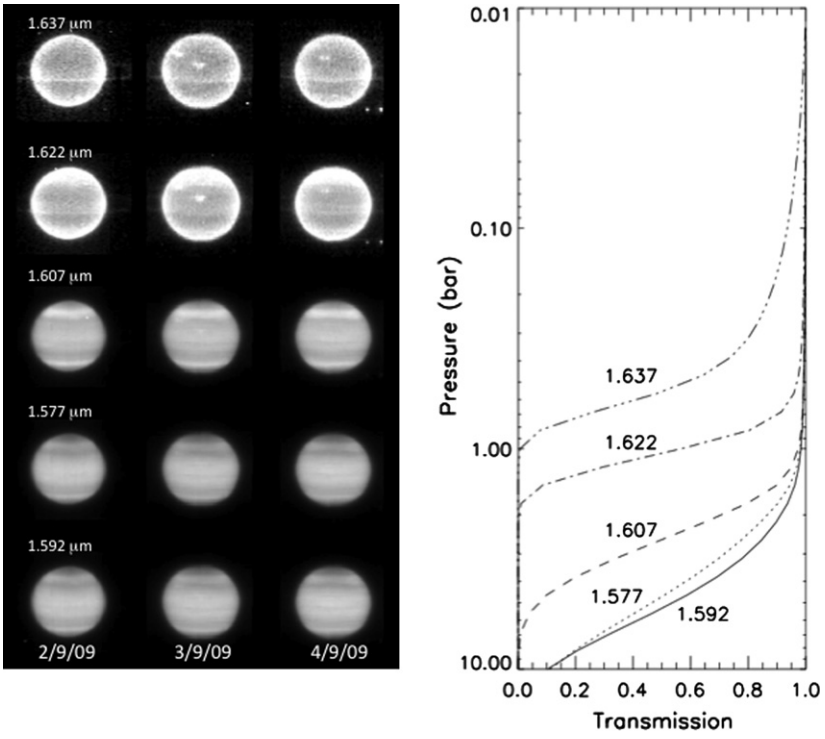

Fig. 3. Recombined Gemini/NIFS observations (left panel) for September 2nd (left column), 3rd (middle column) and 4th (right column) plotted at a number of different wavelengths sounding to deeper and deeper levels in Uranus' atmosphere (1.637, 1.622, 1.607, 1.577, 1.592 μm). The transmission curves (to and from space for nadir viewing) for these wavelengths are plotted in the right hand panel.

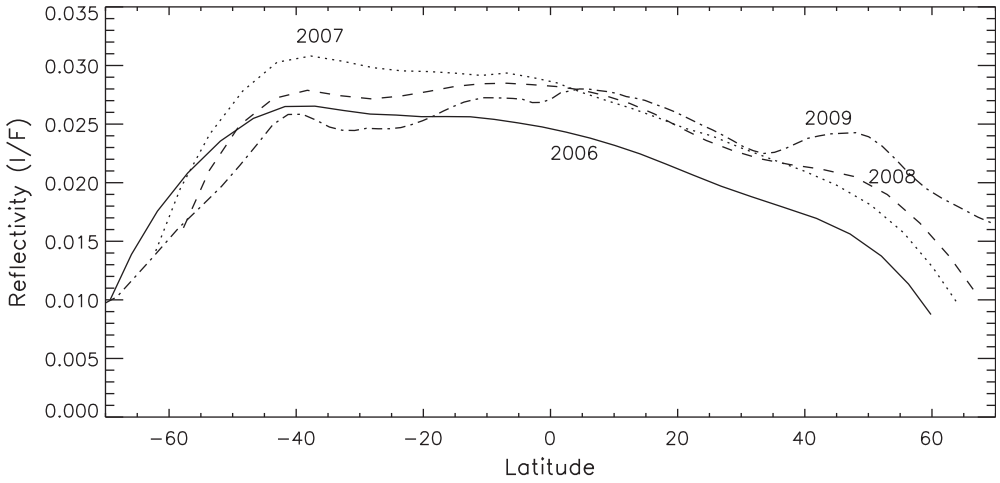

Fig. 4. Central meridian latitudinal I/F variation for 2006–2009 averaged over the UKIRT/UIST H-continuum filter bandpass (1.561–1.583 μm).

of χ^2/n is of the order of 2, indicating a satisfactorily good fit to the measured spectra.

It can be seen from Fig. 5 that in 2009, the northern zone at 45°N was considerably thicker than in previous years and that the zone at 45°S had diminished. In addition, it can be seen that the clouds in the zones at 45°N,S seem to lie at slightly, but significantly lower pressure levels than the clouds at more equatorial latitudes. It is also clear that in 2009, the cloud deck at equatorial latitudes at 2–3 bars appears to have a slight clearing just south of the equator, which can also be seen in the raw J and H-band reflectance data (at wavelengths where the opacity of atmospheric methane is small, Figs. 1–4). This lies very close to the position of Uranus' ε-ring, which can be seen in the CH_4(long) NIRI images (Figs. 1 and 2), in a channel where methane absorbs strongly and thus reflection from Uranus' atmosphere comes only from the thin stratospheric hazes, allowing the ring to be seen clearly. However, it does not coincide completely, as we noted earlier, and so we believe it to be a real tropospheric cloud feature. Fig. 5 also shows a slight thickening in the stratospheric haze at the equator, which can also be seen in the CH_4(long) NIRI images (Figs. 1 and 2). Finally, the retrievals show the tropospheric cloud opacity to be clearing towards the pole for both UKIRT/UIST and Gemini/NIFS observations. With the earlier, lower spatial resolution UKIRT/UIST data it was not absolutely clear if this was partly due to an observational artefact of increased mixing with cold space, but the high spatial resolution of the Gemini data would appear to confirm this latitudinal variation. We also verified that this clearing is not merely due to the sensitivity to deeper cloud variations diminishing with increased zenith angle in our earlier UKIRT analysis (Irwin et al., 2009), where we found that we could probe down to pressures as great as 6 bars, even at the highest emission angles observed.

4. Centre-to-limb observational constraints

Previous reported observations of Uranus by UKIRT/UIST have been limited to the central meridian, where different latitudes are observed at different emission angles and thus where there is some ambiguity in whether we were observing real latitudinal variations or partly geometric variations of the zenith angle and mixing with space. This was one of the main reasons that Gemini/NIFS observations were sought in 2009 since we could then observe latitudes at a range of zenith angles and use the observed limb-darkening or limb-brightening curves at different wavelengths to further refine our vertical cloud structure.

Before we present our Gemini/NIFS results, however, we will report similar observations made in 2008 using the UKIRT/UIST instrument in IFU mode. These data were not reported in our previous papers due to some difficulties in their reduction, which were not solved until recently. Fig. 7 shows the appearance of Uranus at different wavelengths with these data. Observations of the equator were extracted from these data and the spectra measured at different zenith angles fitted simultaneously with NEMESIS to give the cloud profile shown in Fig. 8. For reference, the profile retrieved from the central meridian spectrum alone is also shown. It can be seen that in order to match the observed centre-to-limb curves best, the retrieved cloud deck appears to have a slightly lower pressure, and also appears to have slightly less opacity at pressures between 1.5 and 0.6 bar. However, the differences are small, which given the spatial resolution achievable with the UKIRT IFU observations (Fig. 7) is perhaps not surprising.

The Gemini observations were processed in a similar way. Our previous UKIRT analysis had used a five-point Gauss–Lobatto quadrature scheme (Davis and Polonsky, 1972) in NEMESIS' matrix-operator scattering model (Plass et al., 1973), but to analyse these higher spatial resolution Gemini observations we used instead a nine-point scheme and analysed all the NIFS observed spectra that had the same latitude as that at the centre of the observed disc of Uranus (7°N). At each wavelength, the variation of observed radiance with zenith angle was plotted, smoothed and averaged to yield the mean variation of radiance with zenith angle and then sampled at the quadrature zenith angles. To exclude possible artefacts such as mixing with space near the limb, caused by possible inaccuracies in the geographical registration or our estimate of the effects of seeing on the FOV, we limited our analysis to the first seven zenith angles, giving a maximum zenith angle of 64.3°. The cloud profile retrieved by fitting simultaneously to the measurements at these zenith angles at 7°N is compared with that retrieved from the nadir spectrum alone in Fig. 9. Again we find that by incorporating the centre-to-limb data the main cloud deck is determined to be at much the same pressure level as when retrieving from the nadir observations alone. However, to match the observed limb-darkening curves the retrieved cloud is found to be less vertically extended, with significantly lower opacity in the pressure range 2–0.6 bar. Indeed, considering the vertical smoothing inherent in the continuous cloud opacity retrieval approach employed, the main cloud could be considered to have definite cloud top. This analysis

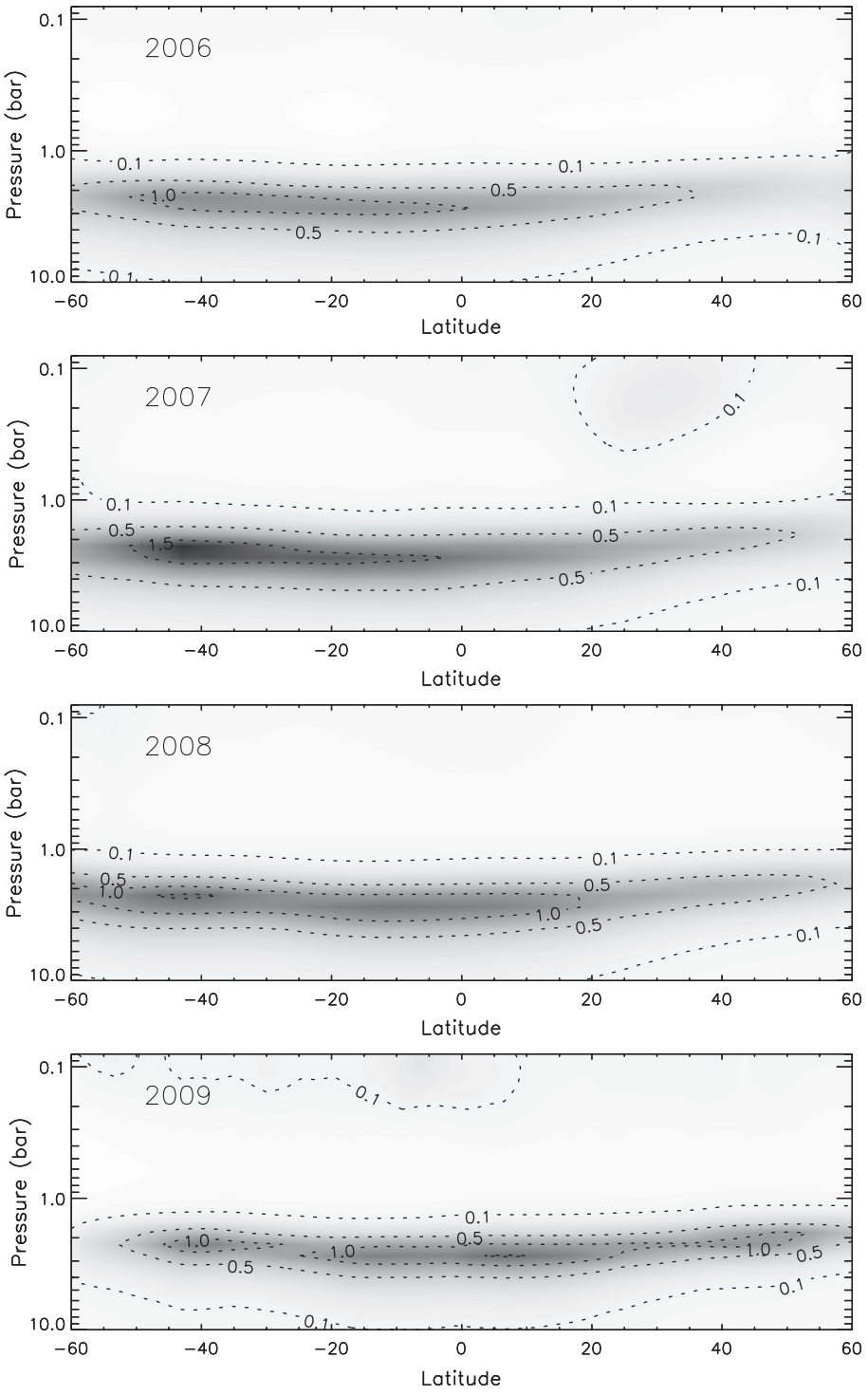

Fig. 5. Retrieved vertical–latitudinal distribution of cloud optical depth per bar (at 1.6 μm) in Uranus' atmosphere from a combination of the UKIRT (2006–2008) and Gemini (2009) observations.

was repeated at a number of other latitudes and we found the same effect on the retrieved vertical cloud structure, although as we move further from the centre of the disc the range of zenith angles observed diminishes rapidly.

The quality of these data also allowed us to validate the cloud particle scattering assumptions we used in our previous analyses of H-band observations, where we assumed a Henyey–Greenstein phase function for the particles with particle asymmetry, $g = 0.7$, and single-scattering albedo, $\bar{\omega} = 0.75$, as recommended by Sromovsky and Fry (2007) from Keck and HST images at a range of wavelengths. Fig. 10 shows how the χ^2 of the fit to the observations at 7°N at zenith angles less than 65° varies with both the assumed particle asymmetry and single-scattering albedo. The optimal solution can be seen to lie along a diagonal line, with the best solution at $g = 0.65$, $\bar{\omega} = 0.75$, very close and indeed hardly distinguishable from the values we have used in all our previous analyses. We also confirmed that these values were suitable at all other latitudes observed.

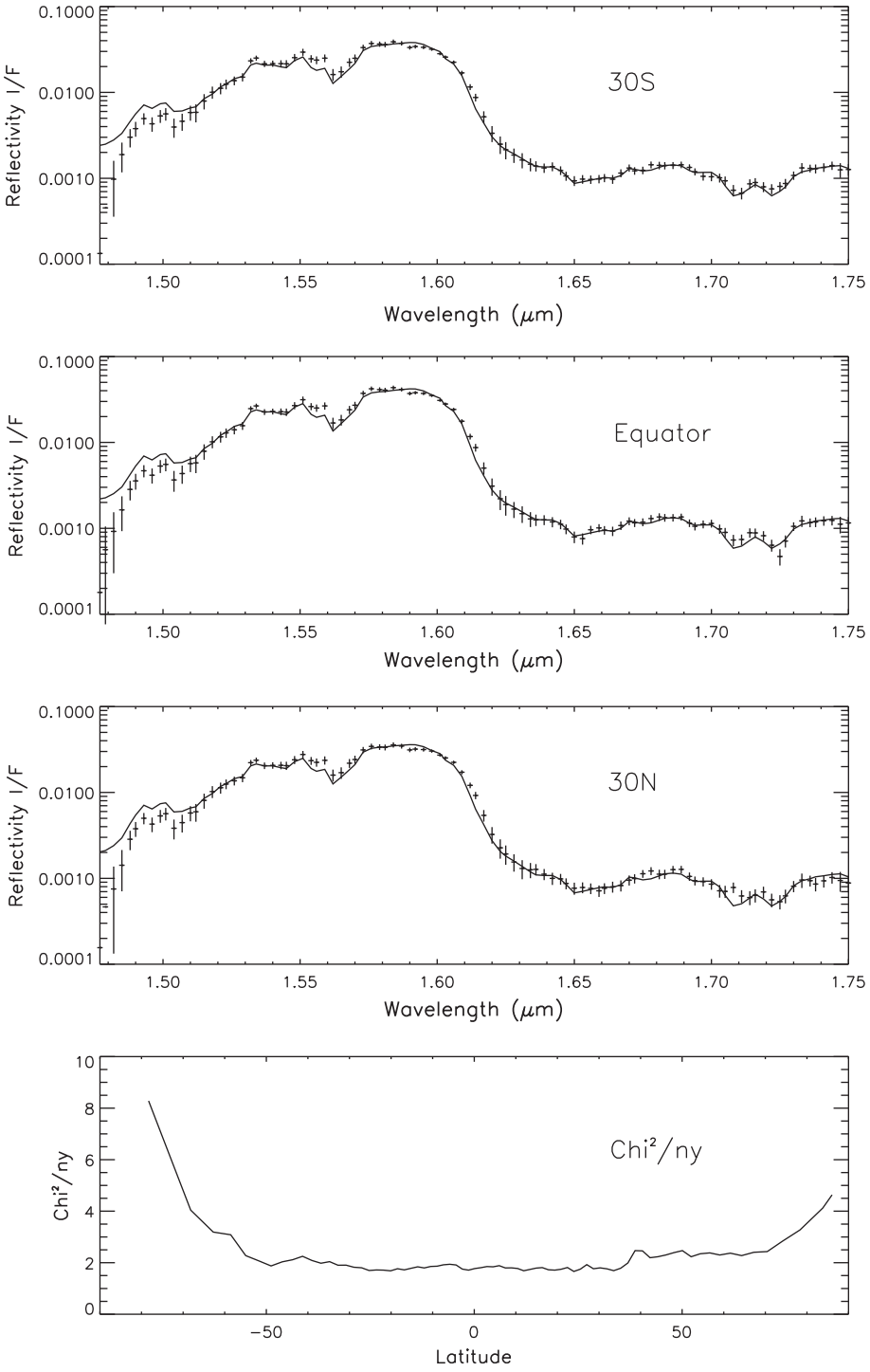

Fig. 6. Fit to the spectra of Uranus observed by Gemini/NIFS in 2009 at three different latitudes together with the overall variation of χ^2/n with latitude.

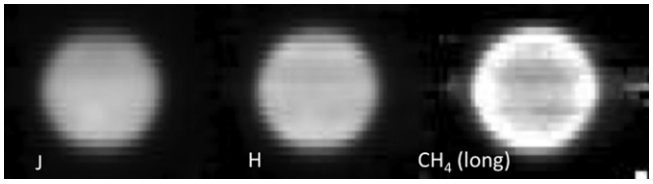

Fig. 7. UKIRT/UIST IFU images of Uranus in several different spectral passbands: 1.55–1.58 μm (left), 1.6–1.68 μm (middle), and 1.7–1.78 μm (right), recorded on 25th July 2008. These observations have a larger pixel size and poorer spatial resolution than the Gemini/NIFS observations.

5. Discrete cloud retrievals

In the second set of NIFS observations on 3rd September 2009 two detached, discrete clouds were seen, one at sub-equatorial latitudes and one near the north polar zone. Individual spectra from these sites were analysed with NEMESIS, using the same wavelength grid and initialisation as for the central-meridian observations; the retrieved cloud opacity profiles are shown in Fig. 11. Here, we can see that the cloud at 15°N lies at a pressure level of 500 mb, while the cloud at 30°N appears more vigorous and reaches a pressure of approximately 200 mb, close to the

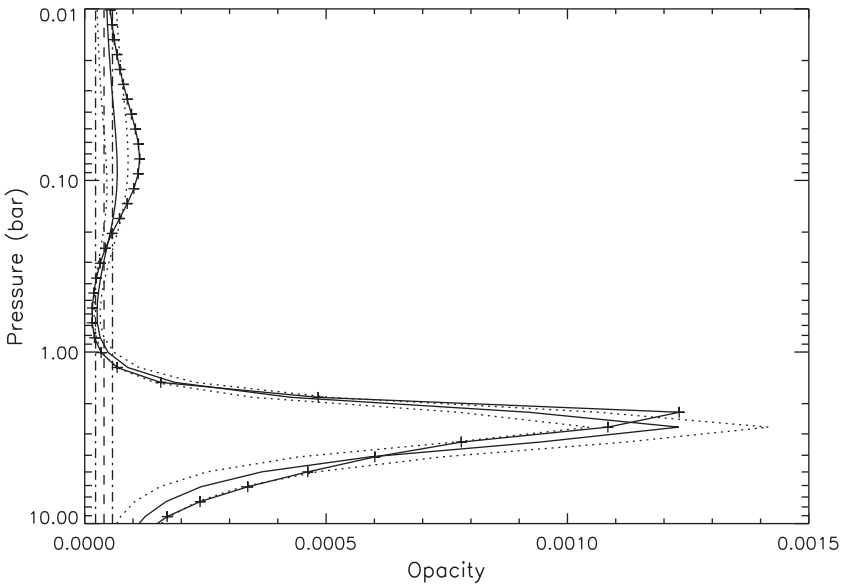

Fig. 8. UKIRT/UIST IFU centre-of-disc and centre-to-limb retrieval of the cloud optical depth per bar (at 1.6 μm) from the observation on 25th July 2008. The profile retrieved from just the central spectrum is plotted as the solid line, with error limits indicated by the dotted lines, while that retrieved simultaneously from a number of zenith angles towards the limb is shown as the solid line with crosses. The a priori cloud optical depth profile and error limits are indicated by the dashed and dashed-dotted lines respectively.

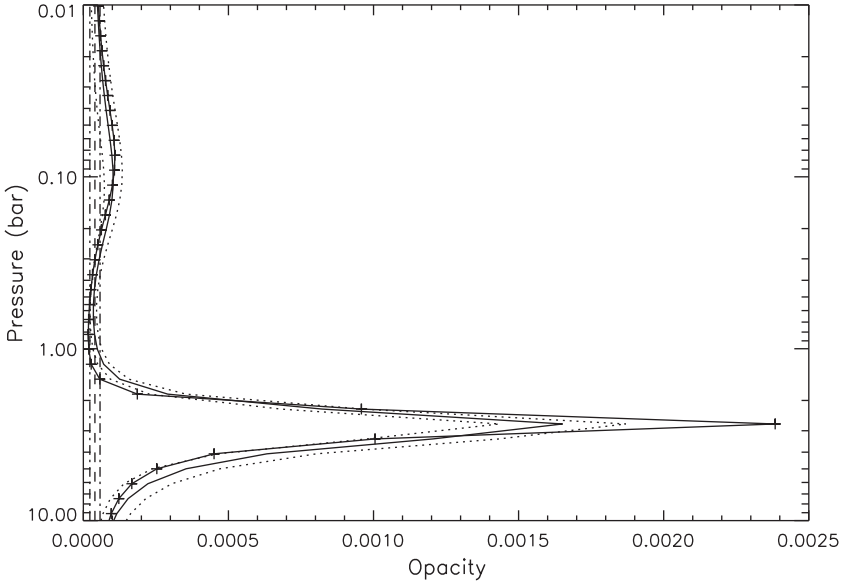

Fig. 9. Retrieved cloud optical depth per bar (at 1.6 μm) from the Gemini/NIFS observations on 2nd September 2009 of the centre-of-disc (7°N) and cloud profile obtained at the same latitude by fitting simultaneously to the observations at zenith less than 65°, plotted using the same plotting scheme as for Fig. 7.

tropopause at 100 mb. Both clouds are vertically separated from the lower main cloud deck, strongly suggesting that they are composed of a different condensate from the main cloud and their high altitude (and thus low assumed temperature) would suggest that they are most likely formed of methane ice.

How such clouds form is unclear; it is generally thought that they form as convective upwellings in regions that are usually convectively stable, but perhaps made conditionally unstable by the absorption of sunlight. Comparison of the 2009 observations with the 2006–2008 data suggests that this activity is perhaps dying down now that the equinox has passed, since these features appear to be far less numerous now than they were in previous years.

6. Simple reflectivity analysis

The Gemini-N/NIFS combined observations of Uranus have approximately 4080 points on disc. To perform individual multiple-scattering retrievals at all positions on the disc would be prohibitively slow on even the most advanced computers. Hence, we have limited ourselves in this study to using our full multiple-scattering retrieval model for (i) discrete clouds, (ii) analysing the central meridian spectra, and (iii) analysing the centre-to-limb observations.

We were, however, interested in exploring whether a more simplistic retrieval scheme could be applied to these data, which would provide similar results along the central meridian, but

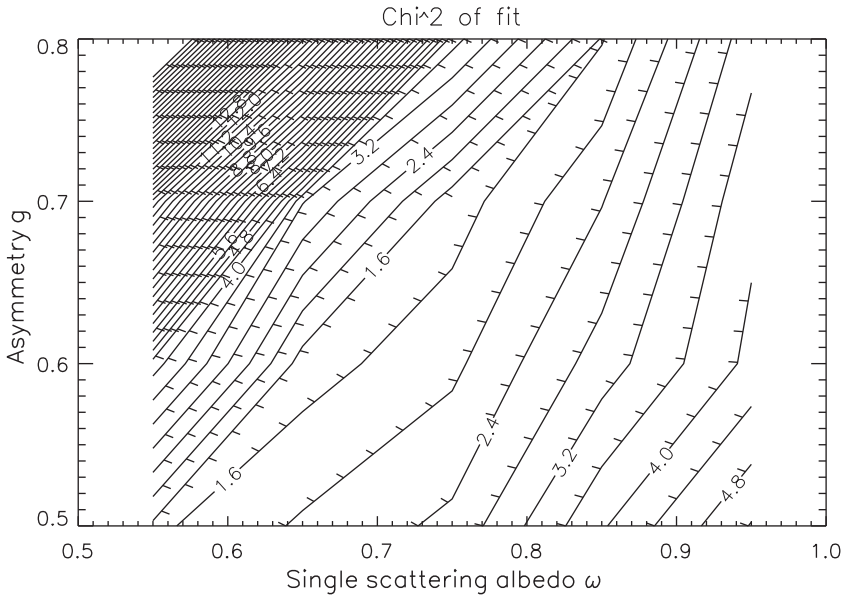

Fig. 10. Quality of fit to the observed Gemini observations at 7°N (i.e. the disc centre) smoothed and interpolated to the first seven zenith angles of the nine-point Gauss–Lobatto quadrature scheme used in our matrix-operator scattering model as a function of assumed particle single-scattering albedo, $\bar{\omega}$, and scattering asymmetry, g, showing the optimal fit to be $g = 0.65$, $\bar{\omega} = 0.7$.

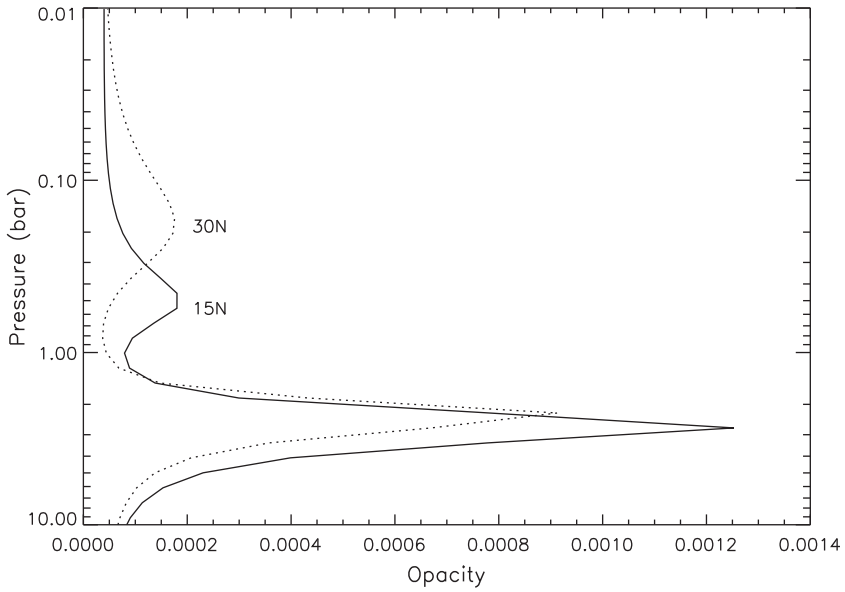

Fig. 11. Retrieved profile of the cloud optical depth per bar (at 1.6 μm) for two discrete, detached clouds observed at 15°N and 30°N on 3rd September 2009 and visible in the central column of Fig. 3. The detached cloud at 15°N appears to lie at a pressure level of 500–600 mbar, while that at 30°N appears to lie at higher altitudes at ~200 mbar.

which would be sufficiently fast to be applied to the entire disc. To this end, we investigated modelling the Uranus' spectrum with a simple reflecting layer model where the total reflectivity observed at a zenith angle, θ, and wavelength, λ, is calculated as:

$$R_{TOT}(\lambda,\theta) = \sum_{i=1}^{M} R_i T_i(\lambda,\theta) \quad (1)$$

where R_i is the reflectivity of the ith level (assumed not to vary with wavelength over this small range) and $T_i(\lambda, \theta)$ is the two-way transmission spectrum from space to that level and back again at a zenith angle, θ, assuming that the difference between the Sun's and observer's zenith angles is negligible, which is reasonable for the case of Uranus as seen from the Earth near opposition. This model is very simplified in that no explicit account is made of the reduction of the incident solar beam by reflection at upper levels, but it has the great advantage of being linear and should be satisfactory for Uranus simulations where the optical depth of hazes above the main cloud deck is small.

The assumed reference Uranus temperature/pressure/abundance profile (Irwin et al., 2010) was split into the same 39 levels as were used in the multiple-scattering retrieval and the two-way transmission spectra to each level calculated with our correlated-k model for a range of zenith angles from 0° to 80° with a step of 10°. The observed reflectivity spectrum was then fitted using this forward model, interpolating the transmission table to the observed zenith angle, and the process of optimal estimation (Rodgers, 2000). Eq. (1) can be written in matrix form as $\mathbf{y} = \mathbf{Kx}$, where $\mathbf{y}$ is the modelled spectrum (at zenith angle, θ), $\mathbf{K}$ is the matrix of the two-way transmissions from space to each level at that angle for

each wavelength, and **x** is the modelled reflectivity at each atmospheric level. Since the assumed forward model is linear, the best-fit vertical reflectivity profile $\hat{\mathbf{x}}$ may be estimated from the measured total reflectivity spectrum, $\mathbf{y}_m$, in one step from optimal estimation theory (Rodgers, 2000) as:

$$\hat{\mathbf{x}} = \mathbf{S}_x\mathbf{K}^T(\mathbf{K}\mathbf{S}_x\mathbf{K}^T + \gamma\mathbf{S}_\varepsilon)^{-1}\mathbf{y}_m \quad (2)$$

where $\mathbf{S}_x$ is the assumed solution correlation matrix of the vertical reflectivity profile, $\mathbf{S}_\varepsilon$ is the correlation matrix of the measured spectrum, and γ is a trade-off parameter used to tune the retrieval. The solution correlation matrix was set to be unity along the leading diagonal with off diagonal elements set to $\exp(-(i-j)^2)$, while the measurement correlation matrix was set to be a unit matrix. Setting the tuning parameter, γ, to be unity resulted in an acceptable level of smoothing (and led to $\chi^2/n \approx 1$) and the retrieval model was applied to the Gemini/NIFS observed spectra at all positions on Uranus' disc for all three days of observation. The retrieved vertical cloud reflectivity profile along the central meridian on 2nd September 2009 is shown in Fig. 12, together with the cloud opacity profile retrieved with the full multiple-scattering model for comparison. The reflectivity profile retrieved by the simple model in just a few seconds is remarkably similar to the opacity profile retrieved by the full multiple-scattering model in several days, although the simple model results in a more vertically extended cloud profile, which also peaks at slightly lower pressures. Bearing these differences in mind, the variation in retrieved cloud reflectivity using this simple model at different pressure levels across the disc of Uranus on all three days observed by Gemini-N/NIFS is shown in Fig. 13. Here we can see that the deeper clouds are limited to latitudes less than about 30–40°, with a reduction in reflection near the equator, while clouds at lower pressures are responsible for the features at ±45°, just as we saw using our full multiple-scattering model. The reduction in reflection from the deeper clouds towards the poles can clearly be seen to be not simply an artefact of the increasing zenith angle towards the poles, since the cloud opacity at these levels extends almost entirely to the East and West limbs.

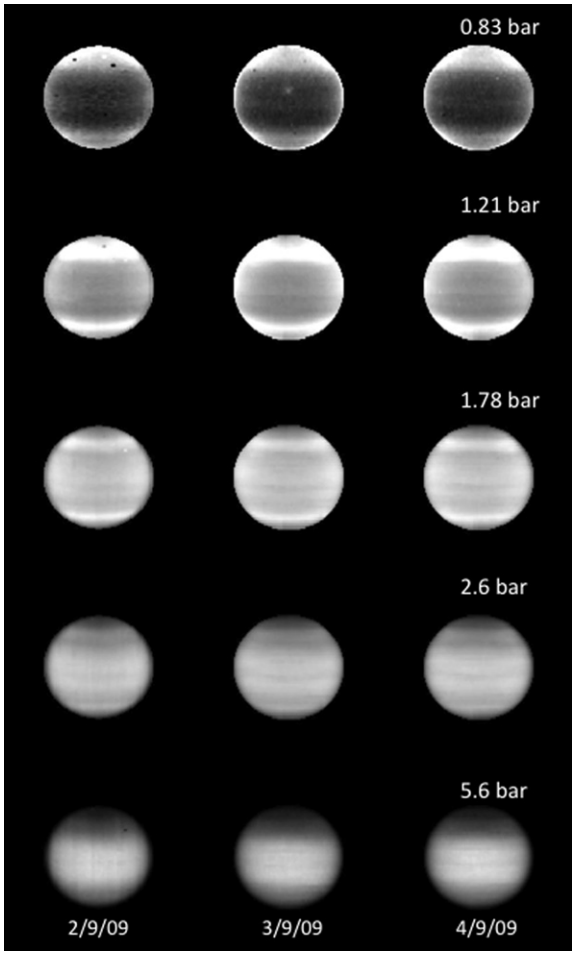

Fig. 13. Retrieved cloud reflectivities using a simplistic cloud reflectivity scheme at the levels: 0.83, 1.21, 1.78, 2.60 and 5.60 bar.

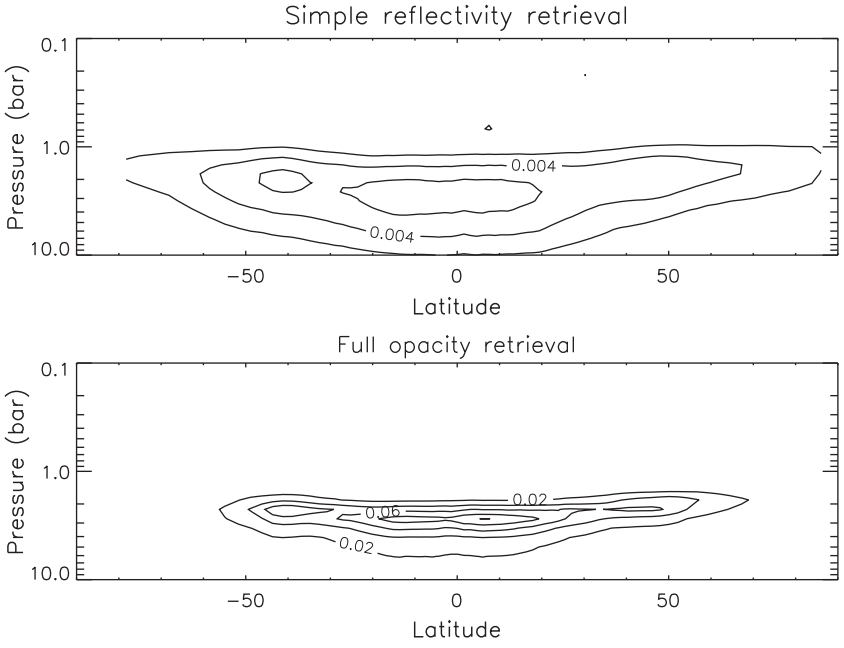

Fig. 12. Comparison between a simple cloud reflectivity retrieval (top) and the full multiple-scattering retrieval (bottom) along the central meridian of the 2nd September 2009 Gemini NIFS observations. The retrieved units in the top plot are the reflectivity of the clouds at different levels, while the units of the bottom plot are cloud optical depth per bar (at 1.6 μm). The basic similarity is clear, although the simplistic retrieval is less well confined, and also peaks at slightly lower pressures.

That such a simple model should yield retrieved vertical cloud structures which bear a striking similarity with those retrieved using a full multiple-scattering model might suggest that the single scattering approximation is appropriate for modelling these data. However, using such a model in NEMESIS we found we were completely unable to fit the observations, even when we assumed a particle single-scattering albedo of unity. The reason for this is that our simplistic reflectivity model makes no account of any radiation removed from the incident solar beam by reflection at upper levels, unlike a single-scattering model, where this effect is fully accounted for. Instead, our simple model is rather more akin to the multiple scattering case we actually observe, where although some solar radiation is reflected to the observer from the upper levels, most is scattered onwards to deeper levels from where it may then be reflected back to the observer relatively unimpeded.

7. Discussion and conclusion

The reflectivity distributions seen in Fig. 13 clearly illustrate that the vertical–latitudinal cloud opacity structure retrieved from these observations has rather different latitude distributions at different pressure levels. This is more clearly seen in Fig. 14 where we have taken cross-sections though the cloud opacity profiles retrieved along the central meridian using the full multiple-scattering model from the September 2nd 2009 Gemini/NIFS observations. These cross-sections have been arbitrarily scaled to allow easy intercomparison between different pressure levels. It can be seen that at deeper levels, the cloud opacity is more confined between 30 and 40°N and S, or in other words that the main cloud deck appears to be at deeper pressure levels at these latitudes. If the determinations of Karkoschka and Tomasko (2009) are correct and the abundance of methane (and thus presumably other volatiles) is higher in this region, then it suggests that convection from the interior is most active at these latitudes and thus that we might expect the cloud condensation levels to be deeper, which would appear to be consistent with these cloud retrievals. This interpretation is also consistent with microwave VLA observations made of Uranus in 2005 (Hofstadter et al., 2009; Orton et al., 2007), which show decreased emission at latitudes less than 45°N,S, consistent with increased levels of volatiles, suggestive of convective overturning. As we move to lower pressures, the latitudinal structure changes markedly, with the bright zones at 45°S and 45°N apparently due to increased cloud opacity in the 1–2 bar level, with the cloud at 45°S appearing to extend to deeper pressures than its counterpart at 45°N. Similar latitudinal variation of cloud opacity at different pressure levels was observed by Sromovsky and Fry (2007) (their Fig. 25) from Keck and HST observations in 2004, by Irwin et al. (2007) from UKIRT observations in 2006, and also by Karkoschka and Tomasko (2009) from HST-STIS observations in 2002. While it is clear that the cloud opacity at pressures less than 2 bars is changing significantly year-by-year, the variation at deeper pressures levels seems to be varying at a somewhat slower rate. The vertical resolution of these observations, even when centre-to-limb observations are analysed, make it difficult to discriminate between whether these features are (i) due to two different distinct cloud levels, as is preferred by Sromovsky and Fry (2007), or (ii) whether they result from a continuous cloud distribution, as has been assumed in our retrieval model. However, the cloud structure at 45°N,S and that nearer the equator do seem sufficiently distinct to wonder if we are in fact seeing two distinct types of clouds, with perhaps methane condensing to form the bright circumpolar zones and another condensate, presumed to be either H_2S or NH_3 condensing to form the deeper, more equatorial clouds. Why there should be apparently no methane cloud over the equatorial regions is curious. It is possible that convection is not strong enough at mid-latitudes to raise methane rapidly enough to its condensation level to form an observable cloud, except in localised regions of rapid convection to form the small clouds seen at mid-latitudes. Alternatively, it may be that methane cloud droplets form so rapidly that methane rains out almost immediately, leaving very little observable cloud density. However, why either of these processes should happen at equatorial and mid-latitudes, and not in the circumpolar zones is unclear. Another curious feature is the slightly darker region seen in the lower cloud deck at the equator. This, together with the darker regions seen just equatorwards of the bright zones at 45°N,S is suggestive of a region of downwelling, which would lower the cloud opacity as it is seen to do on both Jupiter and Saturn. For this to be true, then one might expect upwelling to be strongest between these dark regions, at 20–30°N,S, which is precisely the meridional circulation inferred from Voyager 2 upper tropospheric temperature observations by Read (1987) and Flasar et al. (1987). Such a circulation also provides one explanation of why Uranus has retrograde zonal winds at the equator, since air moving from mid-latitudes to the equator would have to slow its zonal motion in order to conserve angular momentum. However, there do exist other suggested mechanisms for Uranus' retrograde equatorial

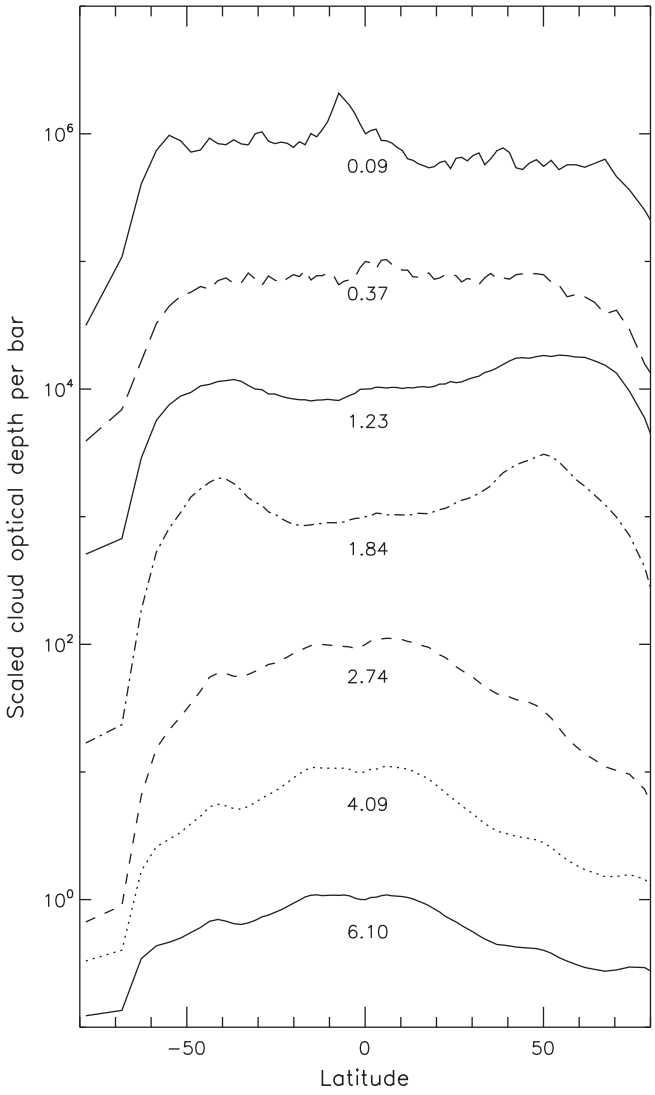

Fig. 14. Cross sections through the retrieved cloud structure from the Gemini/NIFS observations of 2nd September 2009. The numbers indicate the pressure level (bars). The cloud optical depth per bar values have been arbitrarily scaled to allow easy intercomparison between the latitudinal variation at different altitudes. The peak at ~8°S in the 0.09 bar curve is the ε-ring.

zonal winds, including whether the intrinsic heat flux is strong enough for convection at the equator to penetrate to the upper troposphere and generate Rossby waves there (Liu and Schneider, 2010). How the circulation changes nearer the poles is just as mysterious. Radio, microwave and the observations presented here do seem to suggest that the air is generally subsiding polewards of the circumpolar zones at 45°N,S, but the bright clouds seen in the zones themselves, and the marked difference in their apparent altitude compared to the more equatorial clouds suggests that convection is vigorous at these latitudes, and is strongly dependent on the sub-solar latitude and changes almost immediately as the seasons progress. The final curious feature are the small detached clouds seen between 45°N,S, some of which were detected and analysed here, which seem to lie well above the main equatorial cloud deck and be detached from it. Such clouds are presumably formed of CH_4 ice condensing in regions of local vigorous convective uplift. The fact that these have become more active since the Voyager observations would suggest that increased insolation at these latitudes lowers the vertical stability of the upper troposphere, allowing such features to form. Another consideration is that these cloud features are usually small, compact and last for considerable periods of time (Sromovsky and Fry, 2005, 2007). If they were simply the tops of localised convection cells, one might expect them to be quickly disrupted by the latitudinal wind shear seen at these latitudes. The fact that they live so long suggests that they might be stable vortices and since they exist in regions of anticyclonic vorticity, then the similarity with stable anticyclonic vorticities in the atmosphere of Jupiter is intriguing, especially considering that jovian anticyclonic vortices are also observed to have very high cloud tops.

The Gemini-N observations in 2009 clearly show that the seasonal variations in the vertical–latitudinal distribution of cloud opacity observed by a number of authors during Uranus' equinox season has continued, with the northern bright zone at 45°N continuing to brighten, while its counterpart at 45°S continues to fade. During this period, the equatorial zone has increased in brightness, leading to more distinctly discernible darker mid-latitudes. The higher spatial resolution of the Gemini-North observations and the ability to observe the centre-to-limb curves at multiple wavelengths have allowed us to: (1) validate the decrease in cloud opacity of the deeper clouds towards the poles, (2) better constrain the vertical distribution and show that the main cloud deck at 2–3 bars has a well-defined cloud top; and (3) has allowed us to examine the finer latitudinal scale structure and better demonstrate that the clouds at 45°N,S condense at considerably lower pressures than the clouds at more equatorial latitudes, which suggests they may have a different composition, presumably CH_4 ice rather then H_2S or NH_3 in the lower cloud deck. The thin darker region near the equator is curious and seems to be a real cloud feature of unknown genesis, although we suggest it is caused by a narrow region of subduction near the equator. In addition, two small discrete clouds were observed at 15°N and 30°N, which are detached from the main cloud deck and are likely composed of a different condensate, presumably methane ice.

Acknowledgments

We are grateful to the United Kingdom Science and Technology Facilities Council for funding this research and also to our support astronomers: Richard McDermid (2009), Chad Trujillo (2009), Andy Adamson (2007, 2008), Watson Varricattu (2006), and also to Ilona Soechting in the UK Gemini Office. The Gemini Observatory is operated by the Association of Universities for Research in Astronomy, Inc., under a cooperative agreement with the NSF on behalf of the Gemini partnership: the National Science Foundation (United States), the Science and Technology Facilities Council (United Kingdom), the National Research Council (Canada), CONICYT (Chile), the Australian Research Council (Australia), Ministério da Ciência e Tecnologia (Brazil) and Ministerio de Ciencia, Tecnología e Innovación Productiva (Argentina). The United Kingdom Infrared Telescope is operated by the Joint Astronomy Centre on behalf of the Science and Technology Facilities Council of the UK.

References

Alexander, A.F.O., 1965. The Planet Uranus: A History of Observation, Theory, and Discovery. Faber and Faber, London.

Borysow, A., 1991. Modeling of collision-induced infrared absorption spectra of H_2–H_2 pairs in the fundamental band at temperatures from 20 to 300 K. Icarus 92, 273–279.

Borysow, A., 1992. New model of collision-induced infrared absorption spectra of H_2–He pairs in the 2–2.5 micron range at temperatures from 20 to 300 K – An update. Icarus 96, 169–175.

Cavanagh, B., Jenness, T., Economou, F., Currie, M.J., 2008. The ORAC-DR data reduction pipeline. Astron. Nach. 329, 295–297.

Davis, P.J., Polonsky, I., 1972. Numerical interpolation, differentiation and integration. In: Abramowitz, M., Stegun, I.A. (Eds.), Handbook of Mathematical Functions (with Formulas, Graphs, and Mathematical Tables). Dover Publications.

Flasar, F.M., Conrath, B.J., Gierasch, P.J., Pirraglia, J.A., 1987. Voyager infrared observations of Uranus' atmosphere: Thermal structure and dynamics. J. Geophys. Res. 92, 15011–15018.

Hammel, H.B., Rages, K., Lockwood, G.W., Karkoschka, E., de Pater, I., 2001. New measurements of the winds on Uranus. Icarus 153, 229–235.

Hanel, R.A., Conrath, B.J., Flasar, F.M., Kunde, V., Maguire, W., Pearl, J.C., Pirraglia, J., Samuelson, R., Horn, L., Schulte, P., 1986. Infrared observations of the uranian system. Science 233, 70–74.

Hofstadter, M.D. et al., 2009. Infrared and microwave observations of Uranus: Implications for temperature, composition, circulation and a standard calibration model for Herschel. American Astronomical Society, DPS Meeting #41, #28.03.

Irwin, P.G.J., Sromovsky, L.A., Strong, E.K., Sihra, K., Teanby, N.A., Bowles, N., Calcutt, S.B., Remedios, J.J., 2006. Improved near-infrared methane band models and *k*-distribution parameters from 2000 to 9500 cm^{-1} and implications for interpretation of outer planet spectra. Icarus 181, 309–319.

Irwin, P.G.J., Teanby, N.A., Davis, G.R., 2007. Latitudinal variations in Uranus' vertical cloud structure from UKIRT UIST observations. Astrophys. J. 665, L71–L74.

Irwin, P.G.J., Teanby, N.A., de Kok, R., Fletcher, L.N., Howett, C.J.A., Tsang, C.C.C., Wilson, C.F., Calcutt, S.B., Nixon, C.A., Parrish, P.D., 2008. The NEMESIS planetary atmosphere radiative transfer and retrieval tool. J. Quant. Spectrosc. Radiat. Trans. 109, 1136–1150.

Irwin, P.G.J., Teanby, N.A., Davis, G.R., 2009. Vertical cloud structure of Uranus from UKIRT/UIST observations and changes seen during Uranus' Northern Spring Equinox from 2006 to 2008. Icarus 203, 287–302.

Irwin, P.G.J., Teanby, N.A., Davis, G.R., 2010. Revised vertical cloud structure of Uranus from UKIRT/UIST observations and changes seen during Uranus' Northern Spring Equinox from 2006 to 2008: Application of new methane absorption data and comparison with Neptune. Icarus 208, 913–926.

Karkoschka, E., Tomasko, M., 2009. The haze and methane distributions on Uranus from HST-STIS spectroscopy. Icarus 202, 287–302.

Karkoschka, E., Tomasko, M., 2010. Methane absorption coefficients for the jovian planets from laboratory, Huygens, and HST data. Icarus 205, 674–694.

Lindal, G.F., Lyons, J.R., Sweetnam, D.N., Eshleman, V.R., Hinson, D.P., 1987. The atmosphere of Uranus – Results of radio occultation measurements with Voyager 2. J. Geophys. Res. 92, 14987–15001.

Liu, J., Schneider, T., 2010. Mechanisms of jet formation on the giant planets. American Astronomical Society, DPS Meeting #42, #44.03. Bull. Am. Astron. Soc. 42, 1045.

Orton, G.S., Hofstadter, H., Leyrat, C., Encrenaz, T., 2007. Spatially resolved thermal imaging and spectroscopy of Uranus and Neptune. In: Workshop on Planetary Atmospheres Held November 6–7, 2007 in Greenbelt, Maryland. LPI Contribution No. 1376, pp. 93–94.

Plass, G.N., Kattawar, G.W., Catchings, F.E., 1973. Matrix operator method of radiative transfer. 1: Rayleigh scattering. Appl. Opt. 12, 314–329.

Read, P.L., 1987. Clearer circulation on Uranus. Nature 325, 197–198.

Rodgers, C.D., 2000. Inverse Methods for Atmospheric Sounding: Theory and Practice. World Scientific, Singapore.

Sromovsky, L.A., Fry, P.M., 2005. Dynamics of cloud features on Uranus. Icarus 179, 459–484.

Sromovsky, L.A., Fry, P.M., 2007. Spatially resolved cloud structure on Uranus: Implications of near-IR adaptive optics imaging. Icarus 192, 527–557.

Sromovsky, L.A., Fry, P.M., Hammel, H.B., Ahue, W.M., de Pater, I., Rages, K.A., Showalter, M.R., van Dam, M.A., 2009. Uranus at equinox: Cloud morphology and dynamics. Icarus 203, 265–286.

Tody, D., 1993. IRAF in the nineties. In: Hanisch, R.J., Brissenden, R.J.V., Barnes, J. (Eds.), Astronomical Data Analysis Software and Systems II, A.S.P. Conference Ser., vol. 52, 173-183.

Zheng, C., Borysow, A., 1995. Modeling of collision-induced infrared absorption spectra of H_2 pairs in the first overtone band at temperatures from 20 to 500 K. Icarus 113, 84–90.